J. Nonlinear Sci. Vol. 16: pp. 255–281 (2006)
DOI: 10.1007/s00332-005-0691-8

Journal of
Nonlinear
Science

Static Equilibria of Rigid Bodies: Dice, Pebbles, and the Poincaré-Hopf Theorem

P. L. Várkonyi and G. Domokos
Budapest University of Technology and Economics, Department of Mechanics, Materials and Structures, H-1111 Muegyetem rkp. 1-3, Budapest, Hungary
and
Center for Applied Mathematics and Computational Physics, Budapest, Hungary
vpeter@mit.bme.hu
domokos@bagira.iit.bme.hu

Received February 1 , 2005; revised manuscript accepted for publication January 23, 2006
Online publication May 22, 2006
Communicated by J. E. Marsden

Summary. By appealing to the Poincaré-Hopf Theorem on topological invariants, we introduce a global classification scheme for homogeneous, convex bodies based on the number and type of their equilibria. We show that beyond trivially empty classes all other classes are non-empty in the case of three-dimensional bodies; in particular we prove the existence of a body with just one stable and one unstable equilibrium. In the case of two-dimensional bodies the situation is radically different: the class with one stable and one unstable equilibrium is empty (Domokos, Papadopoulos, Ruina, *J. Elasticity* 36 [1994], 59–66). We also show that the latter result is equivalent to the classical Four-Vertex Theorem in differential geometry. We illustrate the introduced equivalence classes by various types of dice and statistical experimental results concerning pebbles on the seacoast.

Key words. Static equilibria, rigid bodies, monostatic bodies, pebble shapes.

MSC numbers. 74G55, 37J05.

1. Introduction

In this paper we study the number and type of static equilibria of homogeneous, convex bodies resting on a horizontal surface without friction in the presence of uniform gravity.

Static equilibria of rigid bodies have been always present in human thought. In particular, the number of *stable* equilibria played a key role: Archimedes provided the first

rigorous method to construct ships with *one* stable equilibrium [7]. Throwing dice (as well as making decisions in gambling) relies essentially on the existence of *several* stable equilibria with disjoint basins of attraction. While classical (cubic) dice have six stable equilibria, an astonishing diversity of other dice exists as well: dice with 2, 3, 4, 6, 8, 10, 12, 16, 20, 24, 30, and 100 stable equilibria appear in various games [8]. The invention of the wheel was essentially equivalent to the realization that a continuum of equilibria can exist. Static equilibria (appearing as fixed points) are also essential in the understanding of the phase space in the dynamics of rolling, which emerges in current research [14], [15] as well as in classical works [16]. Another classical problem is stabilizing unstable equilibria, ever since Christopher Columbus balanced his famous egg (to which story we will return later), and it is still present in current research concerning dynamic stabilization [11], [12], [13].

While many specific examples of solid bodies with a given number of stable equilibria have been demonstrated, bodies with *one* stable equilibrium seem to be of special interest. Such bodies are called *monostatic*, and there are several remarkable related results. It is easy to construct a monostatic body, such as a popular children's toy called "comeback kid" (Figure 1a). However, if we look for *homogeneous*, *convex* monostatic bodies, the task is much more difficult. In fact, one can prove [1] that among planar (slablike) objects *no* monostatic bodies exist, and we will show that this statement is equivalent to the famous Four-Vertex Theorem in differential geometry. The three-dimensional case poses even more difficult questions. Although one can construct a homogeneous, convex monostatic body (cf. Figure 1b), the task is far less trivial if we look for a monostatic polyhedron with a *minimal number* of facets. Conway and Guy [3] constructed such a polyhedron with 19 faces (similar to the body in Figure 1b), it is still believed that this is the minimal number. It was shown by Heppes [6] that no homogeneous, monostatic tetrahedron exists. However, Dawson [4] showed that homogeneous, monostatic simplices exist in $d > 10$ dimensions. More recently, based on Conway's results, Dawson and Finbow [5] showed the existence of monostatic tetrahedra, however, with inhomogeneous mass density.

Bodies with just one stable equilibrium are called monostatic; we will refer to the even more special class of bodies with just one stable and one unstable equilibrium (and

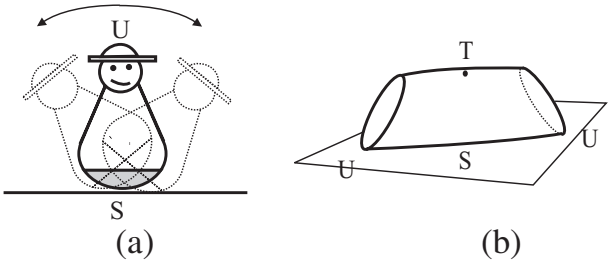

Fig. 1. (a) A toy with one stable and one unstable equilibrium (i.e. an inhomogeneous, mono-monostatic body), called comeback kid. (b) A convex, homogeneous solid body with one stable equilibrium (monostatic body). In both plots, S, T, and U denote points of the surface corresponding to stable, saddle type, and unstable equilibria of the bodies, respectively.

no other equilibria) as "mono-monostatic." While in the case of two-dimensional bodies being monostatic implies being mono-monostatic (and vice versa), the three-dimensional case is more complicated: a monostatic body could have, in principle, any number of unstable equilibria. V. I. Arnold pointed out [17] that the existence of homogeneous, convex mono-monostatic bodies is an interesting question. Although the nonexistence of such objects in two dimensions is known [1], Arnold nevertheless conjectured that their three-dimensional counterparts existed.

Our primary goal is to find a meaningful classification scheme encompassing all possible combinations of equilibria for convex, homogeneous bodies (this will be done in Section 2) and to identify all empty and non-empty classes in this scheme. The backbone of our argument (discussed in Sections 3–5) is simple: we will give an explicit construction for a three-dimensional mono-monostatic body (thus confirming Arnold's conjecture) and deduce the existence of bodies in other classes by complete induction. In the inductive steps, small portions are sliced off the bodies, increasing the number of their equilibria. The same idea appears in the construction of Zocchihedra (dice with 100 facets), which are constructed this way from spheres [8]. Finally, Section 6 summarizes and illustrates the material by showing statistical results on pebbles as well as discussing various shapes of dice.

2. The Global Classification Scheme and Formulation of the Main Statements

In this section we introduce a global classification scheme for convex, homogeneous bodies based on the number and type of their equilibria, and we will use the notations of this scheme to formulate all of our principal claims.

A homogeneous, convex 3D-body can be uniquely defined in a spherical coordinate system as the scalar distance $R(\theta,\varphi)$ measured from the center of gravity G. The singular (fixed) points of the gradient vector field of R correspond to static equilibria: the typical cases are

(1) stable node
(2) unstable node
(3) saddle-type singular points,

corresponding to nondegenerated minima, maxima, and saddle points of $R(\theta, \varphi)$, respectively. Bodies with degenerated singular points are not investigated in this paper.

The case of two-dimensional bodies is more transparent: the distance $R(\varphi)$ is just a function of one variable; minima and maxima of R (i.e. stable and unstable nodes of the gradient flow) always emerge in pairs, saddles do not occur.

Our classification of bodies is based on

Definition 1. We call two convex, homogeneous bodies equivalent if for all listed types the number of singular points is equal.

Hence in the two-dimensional case the number of minima uniquely characterizes an equivalence class:

Definition 2. Class $\{i\}$ ($i = 0, 1, 2, \ldots$) contains all homogeneous, convex, two-dimensional bodies with i stable and i unstable equilibria.

As simple examples we mention the ellipse in class $\{2\}$ and regular n-gons in class $\{n\}$.

In the case of three-dimensional bodies (i.e. in the case of two-dimensional flows), Poincaré indices can be associated with the three listed singularities; the indices are $+1$, $+1$, and -1, respectively [10]. We appeal to the

Poincaré-Hopf Theorem [9]. *The index of a vector field (i.e. the sum of the indices associated with the singularities) with finitely many zeros on a compact, oriented manifold is the same as the Euler characteristics of the manifold, implying that the sum* S *of the Poincaré indices depends only on the topology of the manifold; in the case of a sphere, we have* $S = 2$.

Thus, we have

Definition 3. In three dimensions, class $\{i, j\}$, ($i, j = 0, 1, \ldots$) contains all homogeneous, convex bodies with i stable equilibria (minima) and j unstable equilibria (maxima). (Henceforth we use "stable equilibrium" to refer to a nondegenerate local minimum, "unstable equilibrium" to refer to a nondegenerate local maximum, and "saddle" to refer to a nondegenerate saddle point of R.)

Due to the Poincaré-Hopf Theorem, bodies in class $\{i, j\}$ have $k = i + j - 2$ saddles. As simple examples we mention the general ellipsoid with three different axes in class $\{2, 2\}$, the regular tetrahedron in class $\{4, 4\}$, and the cube in class $\{6, 8\}$. By applying the classification schemes of Definitions 1, 2, and 3, we can now formulate our claims.

The equivalence classes $\{0\}$, $\{0, i\}$, and $\{i, 0\}$ ($i = 0, 1, 2, \ldots$) are trivially empty: our vector field has been derived from a scalar potential; hence it has to contain at least one stable and one unstable node, corresponding to the global maximum and minimum of R. We will concentrate on the nontrivially non-empty classes $\{i\}$ and $\{i, j\}$ with $i, j = 1, 2, \ldots$. In the planar case we already mentioned simple examples for all classes $\{i\}$ with $i > 1$. Class $\{1\}$ is less trivial: our intuition suggests that it may be empty and, in fact, [1] proves

Theorem 1. *Class* $\{1\}$ *is empty.*

That is, convex, homogeneous, rigid, planar *slablike bodies*, resting on a horizontal surface in the presence of a uniform, vertical gravity field have at least two *stable* equilibria (in other words, homogeneous monostatic bodies, and thus homogeneous mono-monostatic bodies, do not exist in two dimensions).

At first sight it is not clear what would be the spatial analogy of Theorem 1: the emptiness of the classes $\{1, 1\}$ (mono-monostatic), $\{1, i\}$ (monostatic), or $\{i, 1\}$ are all candidate statements. As V. I. Arnold pointed out [17], the essence of Theorem 1 is that in two dimensions the minimal number of equilibria is *four*. The only three-dimensional bodies with fewer than four equilibria are the mono-monostatic ones, i.e. class $\{1, 1\}$. (For example, the monostatic body in Figure 1b represents class $\{1, 2\}$, and it has one stable, two unstable, and one saddle-type equilibrium, four equilibria altogether.) Hence

the three-dimensional analogy of Theorem 1 would be the *emptiness of class* {1, 1}. Arnold hinted that a 3-D counterexample, with fewer than four equilibria (i.e. a mono-monostatic body) may nevertheless exist. With our current notation this would mean that class {1, 1} is non-empty.

This idea appears to be rather intriguing since (as we show in Appendix B) Theorem 1 is equivalent to the famous

Four-Vertex (or 4V) Theorem [2]. *The curvature of a simple (not self-intersecting), smooth, convex, closed, planar curve always has at least four local extrema, if its extrema are isolated. (The same statement is true for concave curves too, but it has, to our knowledge, no mechanical analogy.)*

The generalization of the 4V theorem for surfaces is far from trivial: it is not clear what should be the analogy of the planar curvature. Our goal is to show that, at least in this mechanical analogue, the spatial generalization fails: we construct explicit, three-dimensional counterexamples with only two equilibria to prove

Theorem 2. *Class* {1, 1} *is non-empty.*

Thus we confirm Arnold's initial guess. We will proceed in Section 3 by constructing the two-parameter family $R(\theta, \varphi, c, d)$ of smooth, closed surfaces in a spherical (r, θ, φ) polar coordinate system. The intuitive idea behind this construction, as we will point out, is rooted in the proof of Theorem 1. Although the planar argument does not work in 3-D, it helps to prove the opposite statement. The bodies representing class {1, 1} are embedded in this family, and Section 4 defines the intervals of the two parameters c and d associated with them. The existence of appropriate values for c and d is demonstrated analytically, and one solution is determined numerically. Appendix A contains the proof of some lemmas. In Section 5 we will use complete induction (based on the idea of Columbus's egg) to prove the natural generalization of Theorem 2 in the form of

Theorem 3. *Class* $\{i, j\}$ *is non-empty for* $i, j > 0$.

3. Construction of a Surface

In Sections 3 and 4 we provide an explicit construction for a homogeneous, convex, mono-monostatic body, i.e. an element of class {1, 1}. As the first step, in this section we define a suitable two-parameter family of surfaces $R(\theta, \varphi, c, d)$ in the spherical coordinate system (r, θ, φ) of Figure 2 with $-\pi/2 < \varphi < \pi/2$ and $0 \leq \theta \leq 2\pi$, or $\varphi = \pm\pi/2$ and no θ coordinate, while $c > 0$ and $0 < d < 1$ are parameters. The solid, homogeneous body bounded by $R(\theta, \varphi, c, d)$ is denoted by $\mathcal{B}$. In Section 4 we will identify a range of the two parameters where $\mathcal{B}$ is in {1, 1}, i.e. it is convex, homogeneous, and has only two equilibria. Before starting the construction, the proof of the emptiness of class {1} in the planar case is sketched (cf. [1]). This proof does not work it the 3-D case; however, it suggests *how to prove the opposite in 3-D*, i.e., how to construct a representative of class {1, 1}.

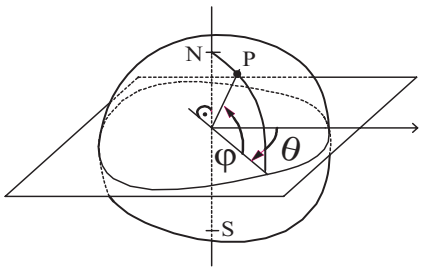

Fig. 2. A P point of the $R(\theta, \varphi)$ surface and the spherical coordinate system.N and S denote the "north pole" and the "south pole" of the surface.

To prove the emptiness of class {1} indirectly, consider a convex, homogeneous planar "body" $\mathcal{B}$ and a polar coordinate system with origin at the center of gravity of $\mathcal{B}$. Let the differentiable function $R(\varphi)$ denote the boundary of $\mathcal{B}$. As demonstrated in [1], nondegenerated stable/unstable equilibria of the body correspond to local minima/maxima of $R(\varphi)$. Assume that $\mathcal{B}$ is in class {1}, i.e., $R(\varphi)$ has only one local maximum and one local minimum. In this case there exists exactly one value $\varphi = \varphi_0$ for which $R(\varphi_0) = R(\varphi_0 + \pi)$; moreover, $R(\varphi) > R(\varphi_0)$ if $\pi > \varphi - \varphi_0 > 0$, and $R(\varphi) < R(\varphi_0)$ if $-\pi < \varphi - \varphi_0 < 0$ (see Figure 3a). The straight line $\varphi = \varphi_0$ (and $\varphi = \varphi_0 + \pi$) passing through the origin O cuts $\mathcal{B}$ into a "thin" ($R(\varphi) < R(\varphi_0)$ and a "thick" ($R(\varphi) > R(\varphi_0)$ part. This implies that *O cannot be the center of gravity*, i.e., it contradicts the initial assumption.

Similar to the planar case, a 3-D body in class {1, 1} can be cut into a "thin" and a "thick" part by a closed curve on its boundary, along which $R(\theta, \varphi)$ is constant. If this separatrix curve happens to be planar, its existence leads to contradiction (if, for

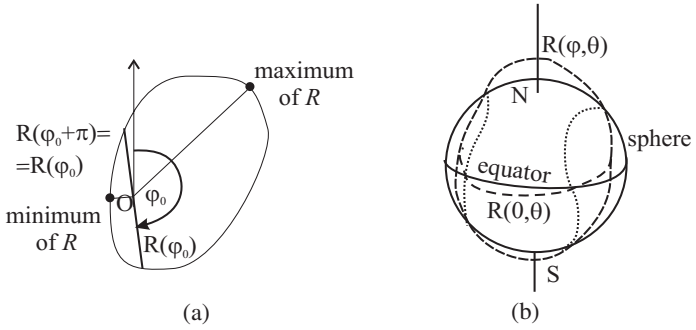

Fig. 3. (a) Example of a convex, homogeneous, planar body bounded by $R(\varphi)$. If R has only two local extrema, the body can be cut into a "thin" and a "thick" half by the line $\varphi = \varphi_0$. Its center of gravity is on the "thick" side; in particular, it cannot be in O. (b) A 3-D body (dashed line) cut into a "thin" and a "thick" half by a tennis ball-like space curve (dotted line) along which $R = R_0$. The continuous line shows a sphere of radius R_0, which also contains this curve.

example, it is the "equator" $\varphi = 0$ and $\varphi > 0/\varphi < 0$ are the thick/thin halves, the center of gravity should be on the upper ($\varphi > 0$) side of the origin). However, in the case of a generic, spatial separatrix the above argument does not apply any more. In particular, the curve can be similar to the ones on the surfaces of tennis balls (Figure 3b). In this case the "upper" thick ("lower" thin) part is partially below (above) the equator; thus it is possible to have the center of gravity at the origin. Our construction will be of this type.

Conveniently, R can be decomposed in the following way:

$$R(\theta, \varphi, c, d) = 1 + d \cdot \Delta R(\theta, \varphi, c), \tag{1}$$

where ΔR denotes the type of deviation from the unit sphere. "Thin"/"thick" parts of the body are characterized by negativeness/positiveness of ΔR (i.e., the separatrix between the thick and thin portions will be given by $\Delta R = 0$), while the parameter d is a measure of the "flatness" of the surface. We will chose adequately small values of d *to make the surface convex*.

Our next goal is to define a suitable function ΔR. We will have the maximum/minimum points of ΔR ($\Delta R = \pm 1$) at the north/south pole ($\varphi = \pm\pi/2$). The shapes of the thick and thin portions of the body are controlled by the parameter c: for $c \gg 1$ the separatrix will approach the equator; for smaller values of c the separatrix will become similar to the curve on the tennis ball.

Consider the following smooth, one-parameter mapping $f(\varphi, c)$: $(-\pi/2, \pi/2) \to (-\pi/2, \pi/2)$:

$$f(\varphi, c) = \pi \cdot \left[\frac{e^{\left[\frac{\varphi}{\pi c} + \frac{1}{2c}\right]} - 1}{e^{1/c} - 1} - \frac{1}{2} \right]. \tag{2}$$

For very large values of the parameter ($c \gg 1$), this mapping is almost the identity; however, if c is close to 0, the deviation from linearity is large (cf. Figure 4).

Based on f, we define the related maps (Figure 5):

$$f_1(\varphi, c) = \sin(f(\varphi, c)), \tag{3}$$

$$f_2(\varphi, c) = -f_1(-\varphi, c). \tag{4}$$

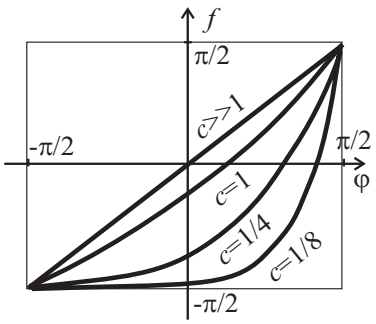

Fig. 4. The $f(\varphi)$ function at some values of c.

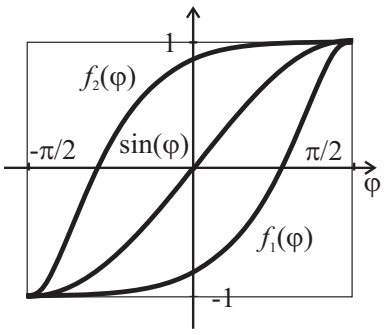

Fig. 5. The $f_1(\varphi)$, $f_2(\varphi)$, and $\sin(\varphi)$ functions at $c = 1/3$.

These two functions are used to obtain

$$\Delta R(0, \varphi, c) = \Delta R(\pi, \varphi, c) = f_1(\varphi, c), \tag{5}$$

$$\Delta R(\pi/2, \varphi, c) = \Delta R(3\pi/2, \varphi, c) = f_2(\varphi, c). \tag{6}$$

The planes $\varphi = 0$ and $\varphi = \pi/2$ will provide two planes of symmetry of the separatrix of Figure 3b; a big portion of section (5) of $\mathcal{B}$ lies in the thick part, while the majority of section (6) is in the thin part. The function

$$a(\theta, \varphi, c) = \frac{\cos^2(\theta) \cdot (1 - f_1^2)}{\cos^2(\theta)(1 - f_1^2) + \sin^2(\theta) \cdot (1 - f_2^2)} = \frac{1}{1 + \tan^2(\theta) \frac{\cos^2(f(\varphi,c))}{\cos^2(f(-\varphi,c))}}, \quad \text{where } |\varphi| < \pi/2, \tag{7}$$

(illustrated in Figure 6) is used to construct ΔR as a "weighted average"-type function

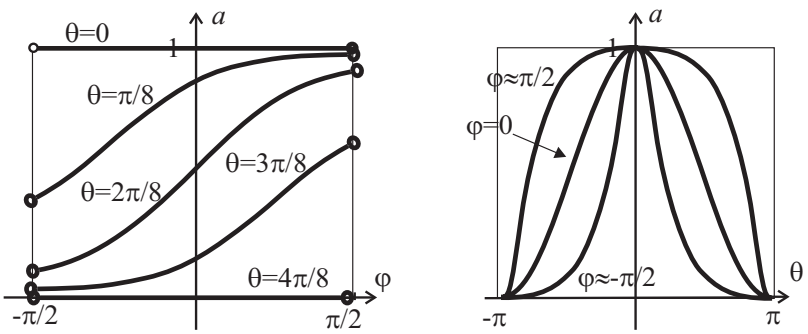

Fig. 6. Sections of the $a(\theta, \varphi)$ function at $c = 1$.

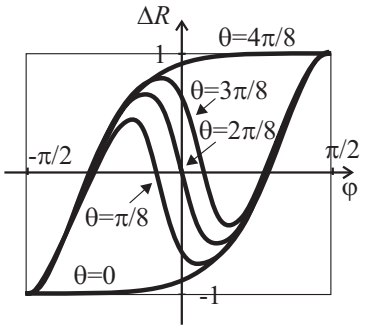

Fig. 7. Sections of the $\Delta R(\theta, \varphi)$ function at constant values of θ; $c = 1/4$.

of f_1 and f_2 in the following way (cf. Figure 6):

$$\Delta R(\theta, \varphi, c) = \left\{ \begin{array}{cc} a \cdot f_1 + (1-a) \cdot f_2 & \text{if } |\varphi| < \pi/2 \\ 1 & \text{if } \varphi = \pi/2 \\ -1 & \text{if } \varphi = -\pi/2 \end{array} \right\}. \tag{8}$$

The choice of the function a ensures on the one hand the gradual transition from f_1 to f_2 if θ is varied between 0 and $\pi/2$; on the other hand, it was chosen to result in the desired shape of thick/thin halves of the body (illustrated in Figure 3b).

The function R defined by equations (1)–(8) is illustrated in Figure 8 for intermediate values of c and d. Before we identify suitable ranges of the parameters where the corresponding body $\mathcal{B}$ is convex and mono-monostatic (Section 4), let us briefly comment on the effect of c. For $c \gg 1$, the constructed surface $R = 1 + d\Delta R$ is separated by the $\varphi = 0$ equator into two unequal halves: the upper ($\varphi > 0$) half is "thick" ($R > 1$) and the lower ($\varphi < 0$) half is "thin" ($R < 1$). By decreasing c, the line separating the "thick" and "thin" portions becomes a space curve; thus the thicker portion moves downward and the thinner portion upward. As c approaches zero, the upper half of the body becomes thin and the lower one becomes thick (cf. Figure 9).

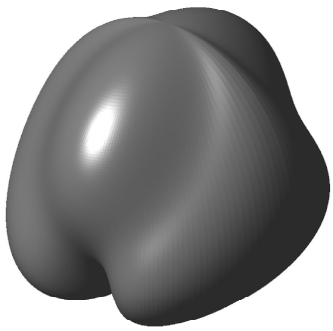

Fig. 8. Plot of $\mathcal{B}$ if $c = d = 1/2$.

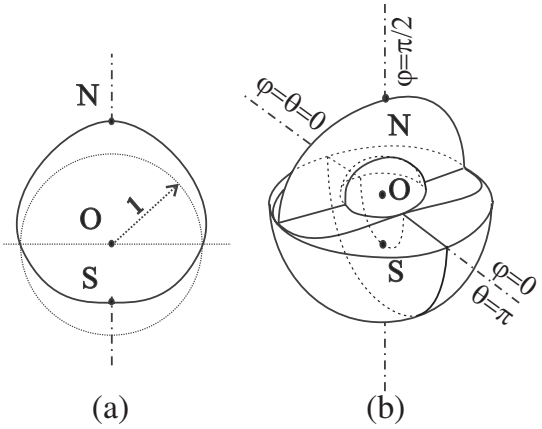

Fig. 9. (a) Side view of $\mathcal{B}$ if $c \gg 1$ (and $d \approx 1/3$). Note that $\Delta R > 0$ if $\varphi > 0$ and $\Delta R < 0$ if $\varphi < 0$. (b) Spatial view of $\mathcal{B}$ if $c \ll 1$. Here, $\Delta R > 0$ typically for $\varphi < 0$ and vice versa.

4. Calibration of the Parameters and the Main Result

In this section we identify the suitable ranges of the parameters c and d where the body $\mathcal{B}$ is convex and has only two equilibria; thus we complete the proof of Theorem 2.

As already mentioned in the introduction, if the center of gravity G of a convex body $\mathcal{B}$ (bounded by the surface R) is at the origin of the spherical coordinate system, then singular points of R correspond to equilibria of the body in a mutually one-to-one manner: those and only those positions are equilibria where one of the singular points is in contact with the underlying surface. The planar analogue of this statement has already been utilized in the proof of Theorem 1 (cf. [1]) and the spatial extension is rather straightforward, so we do not discuss it here. We merely note that *singular points* of R in the spatial case are defined by the conditions

$$\frac{\partial R(\theta, \varphi, c, d)}{\partial \varphi} = \frac{\partial R(\theta, \varphi, c, d)}{\partial \theta} = 0, \tag{9}$$

except at the "poles" ($\varphi = \pm\pi/2$), where the corresponding condition is

$$\left.\frac{\partial R(\theta, \varphi, c, d)}{\partial \varphi}\right|_{\varphi=\pm\pi/2} = 0, \quad \text{for any } \theta. \tag{10}$$

We show in Lemma A.1 (Appendix A) that the function R, defined in equations (1)–(8) of the previous section, has no more than two singular points, namely the poles N and S (cf. Figure 2).

In the forthcoming part of this section we show that $\mathcal{B}$ has the desired properties at appropriate values of the parameters: c and d can be chosen in such a way that

- the center of gravity G coincides with the origo O of the coordinate system, and
- $\mathcal{B}$ is convex.

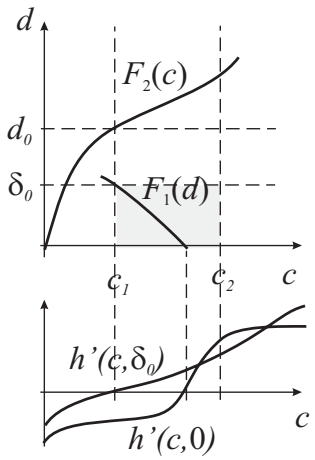

Fig. 10. Illustration for the proofs of Theorem 2 and Lemma A.2.

Lemma A.2 (Appendix A) demonstrates the existence of the positive constants $c_1 < c_2$, δ_0 and of the function F_1, such that for arbitrary $\delta < \delta_0$ there is at least one value $F_1(\delta)$ inside the open interval (c_1, c_2), for which $c = F_1(\delta)$ and $d = \delta$ implies $G \equiv O$. Lemmas A.1 and A.2 (Appendix A) together prove that $\mathcal{B}$ has exactly two equilibria at the parameter values $(c, d) = (F_1(\delta), \delta)$.

As mentioned above, convexity of $\mathcal{B}$ is required to establish a one-to-one correspondence between surface points and possible positions of resting on a horizontal plane. Lemma A.3 (Appendix A) proves that there exists a continuous, positive function $F_2(c) > 0$ for any $c > 0$ such that $\mathcal{B}$ is convex whenever $d < F_2(c)$.

Based on Lemmas A.1, A.2, and A.3 we now proceed to prove Theorem 2. Before doing so, we briefly illustrate the geometric idea. For the sake of visualization we will assume the continuity of the function $F_1(d)$; however, the proof does not rely on this fact. In essence we will show that drawn in the $[c, d]$ plane, a segment or all of the curve $F_1(d)$ $(d < \delta_0)$ is below the $F_2(c)$ line (assuming that d is on the vertical axis). This configuration is illustrated in the upper part of Figure 10. All points of this segment identify surfaces R, which are convex, and the corresponding body $\mathcal{B}$ has only two equilibria. The lower endpoint of this segment is at $(c, d) = (F_1(0), 0)$. We will prove that there exists a finite box (cf. the grey domain of Figure 10) that contains this endpoint; simultaneously, all points inside the box are below the curve $F_2(c)$. All points of $F_1(d)$ inside this finite box are valid solutions, satisfying the statement of Theorem 2.

Proof of Theorem 2. Since $F_2(c) > 0$ is continuous, it has a global minimum $d_0 > 0$ on the closed interval $[c_1, c_2]$ according to the Extreme Value theorem [22]. If $d < \min[\delta_0, d_0]$ and $c = F_1(d)$, then, based on Lemmas A.2 and A.3, $\mathcal{B}$ is convex and its center of gravity is at the origin. Due to Lemma A.1 $\mathcal{B}$ is a convex homogeneous body with only two static equilibria, so homogeneous, convex, mono-monostatic bodies exist and class $\{1, 1\}$ is non-empty. □

Numerical analysis shows that d must be very small ($d < 5 \cdot 10^{-5}$) to satisfy convexity together with the other restrictions, so the created object is very similar to a sphere. (In the admitted range of d the other parameter is approximately $c \approx 0.275$.) This shows that physical demonstration of such an object might be problematic. Nevertheless, other such bodies, rather different from the sphere, may exist; it is an intriguing question what is the maximal possible deviation from the sphere.

We remark that [1] also demonstrates the statement analogous to Theorem 1 for closed, homogeneous, planar *thin wires*. The 3-D analogue for convex, homogeneous spatial *thin shells* is again false, which can be proven in the same way as Theorem 2.

5. The Egg of Columbus and Complete Induction

According to some accounts, Christopher Columbus attended a dinner given in his honor by a Spanish gentleman. Columbus asked the gentlemen in attendance to make an egg stand on one end. After the gentlemen successively tried to and failed, they stated that it was impossible. Columbus then placed the egg's small end on the table, breaking the shell a bit, so that it could stand upright. Columbus then stated that it was "the simplest thing in the world. Anybody can do it, after he has been shown how!" The egg of Columbus has become a metaphor for natural simplicity. In this section we prove Theorem 3 by induction. Our inductive argument is as simple as the egg of Columbus—and not just metaphorically.

Theorem 2 (proven in the previous sections) asserts the non-emptiness of class $\{1, 1\}$. Assume that class $\{i, j\}$ is non-empty. If we can find a way to add one minimum while keeping the number of maxima constant (and vice versa) by small perturbations not violating the convexity of the body, then the non-emptiness of all classes $\{i + 1, j\}$ and $\{i, j + 1\}$ $(i, j > 0)$, and thus Theorem 3 is proven. The first, naive interpretation of the Columbus story is that he *turned* an unstable equilibrium point into a stable one. However, a closer look at the egg reveals that Columbus did something more complex. Based on the superficial account, we cannot decide which of the following scenarios were actually realized (supposing that the egg had a perfect rotational symmetry):

(i) If Columbus hit the table with the egg so that the symmetry axis of the egg was exactly vertical, then by breaking the shell at the unstable equilibrium point (maximum) he produced a small flat area containing one stable equilibrium point in the middle and a circle of degenerated balance points at the borderline of the flat part. This scenario is illustrated in Figure 11b.

(ii) If the axis was somewhat tilted, then by breaking the shell at the unstable equilibrium point (maximum), he produced a small flat area containing one stable equilibrium point (minimum) inside the flat part and one saddle and a maximum at the borderline. This scenario is illustrated in Figure 11c.

Needless to say, scenario (ii) is exactly what we need to produce an additional stable equilibrium without creating new maxima. Since Columbus's algorithm applies only for a degenerate maximum with rotational symmetry, we will use a slightly different technique to produce additional maxima and minima one by one in the vicinity of typical equilibrium points.

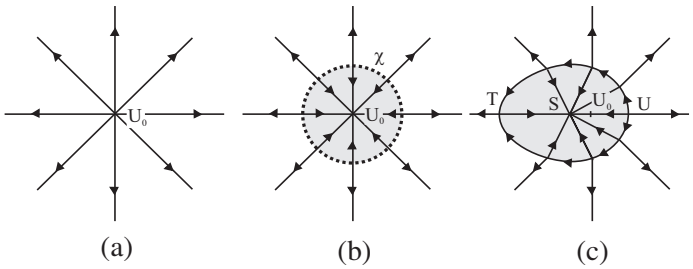

Fig. 11. Analysis of the egg of Columbus. (a) Gradient flow on the original egg near the tip U_0 (unstable equilibrium point). (b) Hitting the table with vertical egg axis: modified flow containing one minimum at U_0 and a set χ of degenerated equilibria. (c) Hitting the table with slightly tilted egg axis: modified flow containing one minimum (S), one saddle (T), and one maximum (U). Grey indicates the flat part of the egg.

5.1. Increasing the Number of Stable Equilibria by One

Consider a (smooth) stable equilibrium point (local minimum) S_0 of the surface R and a point S_1 on the $R = R(S_0)$ sphere, by distance $\delta \ll 1$ from S_0 (Figure 12a). The tangent plane of this sphere at S_1 divides $\mathcal{B}$ into two parts, and we remove the small cap. The modified function R, corresponding to the truncated body, still has a local minimum at S_0 and a new local minimum at S_1. A new saddle point T also emerges, which is a straightforward consequence of the Poincaré-Hopf theorem. This situation is illustrated in Figure 12a, and the gradient flow is shown for the unperturbed and perturbed body in Figures 13a and 13b, respectively.

Notice that the truncation of the body moves the center of gravity G of $\mathcal{B}$ (and thus all nondegenerate critical points) by $\varepsilon \leq o(\delta^4)$, so this effect can be neglected. It is also worth mentioning that the truncated body is only weakly convex, because of its flat part. Strong convexity can be restored by an adequate, arbitrary small perturbation of R.

5.2. Increasing the Number of Unstable Equilibria by One

Again, consider a stable equilibrium point S_0. Draw a very flat cone of revolution ($\delta \ll 1$, see Figure 12b), with rotation axis GS_0 and its peak at S_0. The cone again cuts B into two parts, and we again remove the small one. The modified function R has a local maximum in S_0; it decreases radially until it reaches a circle χ of nonisolated equilibria and beyond the circle, it increases again (see Figure 12b, Figure 13c).

The effect of the deviation of G on the number and type of equilibria can again be neglected if δ is small, with the exception of χ, which is degenerated and structurally unstable. Typically, G' is off the GS_0 line; in this case χ breaks up into one isolated minimum S_1 and a saddle point T (see Figure 13d, Figure 12b). (In the nontypical case when G' happens to be on the line GS_0, χ is preserved; however, it can be broken up into a minimum and a saddle point by an adequate small perturbation of R.) Finally we have one stable (S_1), one saddle (T), and one unstable equilibrium (S_0) instead of the original stable point S_0.

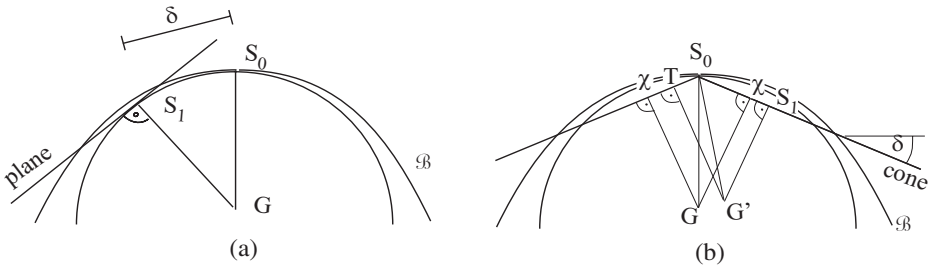

Fig. 12. (a) Illustration of the generalized Columbus algorithm, generating one stable equilibrium point: section of $\mathcal{B}$ in the GS_0S_1 plane, where G denotes the center of gravity of the body. S_1 is a new stable balance point. The newly emerging saddle point T is typically out of this plane. (b) Illustration of the algorithm, generating one unstable equilibrium point: section of $\mathcal{B}$ in the GS_0G' plane. After truncation by the cone, S_0 becomes local maximum. Two points (indicated by χ) of the emerging circle of degenerated balance points χ fall into the represented plane. Due to the deviation of G to G', the circle breaks up to the saddle point T and the stable equilibrium S_1, both of which lie in GS_0G'.

Again the truncated body is weakly convex, and strong convexity can be restored by a further small perturbation of R. If several new equilibria are generated, this should be performed every time: S_1 can be used as the initial stable balance point at the repeated equilibrium-multiplying algorithm, so it should not be weakly convex.

5.3. Completing the Proof of Theorem 3

In Section 5.2 we showed how convex bodies in class $\{i+1, j\}$ and class $\{i, j+1\}$ can be generated by using a body of class $\{i, j\}$. Since Theorem 2 proved the non-emptiness of class $\{1, 1\}$, we now showed that none of the classes $\{i, j\}$, $i, j > 0$ are empty. □

6. Summary

In this paper we revealed a remarkable difference between two-dimensional (slablike) and three-dimensional bodies: while the former have at least four equilibrium points, the latter may have just two. The first statement (Theorem 1) was proven earlier in [1], the latter (Theorem 2) confirms a conjecture of V. I. Arnold. We also proposed a classification scheme for convex, homogeneous bodies, based on the number and type of their static equilibria. This scheme, based on the Poincaré-Hopf theorem, not only helped to formulate and organize the results, it also led to Theorem 3 stating in essence that three-dimensional, homogeneous bodies with arbitrary, prescribed numbers of stable and unstable equilibria exist.

As mentioned in the introduction, the existence of *monostatic* polyhedra with a minimal number of faces has been investigated in the mathematical community [4], [5], [6]. Theorem 3 suggests an interesting generalization of this problem to the existence of polyhedra *in class* $\{i, j\}$, with a minimal number of faces. Intuitively it appears to be evident that polyhedra exist in each class: if we construct a sufficiently fine triangulation

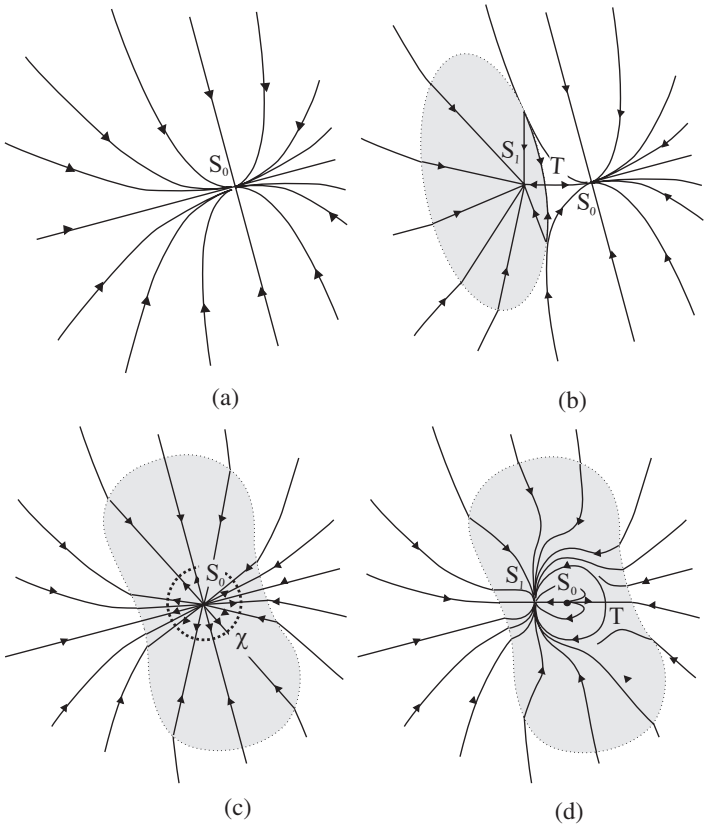

Fig. 13. Gradient flow of R on the surface of B. (a) Small vicinity of a local minimum S_0 of R. (b) The body is truncated along a plane. A second minimum S_1 and a saddle point T occur. (c) The body is truncated along a cone. S_0 becomes a local maximum, and a circle χ of nonisolated singular points emerges on the cone. (d) The deviation of the center of gravity perturbs R. The structurally unstable circle typically breaks up to a minimum S_1 and a saddle point T. Grey indicates the truncated part of the surface.

on the surface of a smooth body in class $\{i,\ j\}$ with vertices at unstable equilibria, edges at saddles and faces at stable equilibria, then the resulting polyhedron will—at sufficiently high mesh density and appropriate mesh ratios—"inherit" the class of the approximated smooth body. It also appears to be true that if the topological inequalities $2i \geq j + 4$ and $2j \geq i + 4$ are valid, then we can have "minimal" polyhedra, where the number of stable equilibria equals the number of faces, the number of unstable equilibria equals the number of vertices, and the number of saddles equals the number of edges. Much more puzzling appear to be the polyhedra in classes *not satisfying* the above topological inequalities: a special case of these polyhedra are monostatic ones; however, many other types belong here as well. In particular, it would be of special interest to know the minimal number of faces of a polyhedron in class $\{1, 1\}$.

The relationship between mathematical proof of existence and the physical world is far from trivial. In some cases the *physical existence* of solutions seems to be evident; nevertheless it is extremely hard to prove existence in the mathematical model, as is the case with the Navier-Stokes equations [21]. Our problem appears to be of the opposite character: the presented mathematical proof was not long, nor did it require complicated tools. Nevertheless, physical intuition fails in this problem. Our experience strongly suggests that all convex, homogeneous bodies have at least two stable equilibria and thus four equilibria altogether. Where does this intuition originate? In the introduction we mentioned *dice* as the probably earliest manmade objects the essence of which is to possess discrete, *multiple* stable equilibria. As games evolved, a large variety of dice have been fabricated, several ones being regular platonic solids or direct descendants thereof. Traditionally, dice having only one stable equilibrium were regarded as illegal (inhomogeneous), called "*loaded*" or "*gaffed*." It is a difficult mathematical challenge to construct a loaded tetrahedral die that is monostatic; this problem is addressed by Dawson and Finbow [5].

Not only manmade objects have the property of often possessing multiple stable equilibria. There exist objects in nature in abundant numbers that probably come closest to the mathematical abstraction of a convex, homogeneous body: pebbles on the seacoast. Pebbles are divided into four groups based on their morphology [18]:

1. oblate (ellipsoidal disk)
2. equant (sphere)
3. bladed (circular disk)
4. prolate (roller, rod).

All these groups can be regarded as limit shapes, resulting from multimillion-year abrasion processes during which pebbles become increasingly smooth; in geological terms, their *roundness* is growing [19]. Apparently, the morphology groups 1 and 3 contain *flat* pebbles with at least two stable equilibria, and group 4 has at least two unstable equilibria, so mono-monostatic bodies of class {1, 1} can be found only in group 2, among "spherical" objects. This is in good agreement with Sections 3 and 4, where we constructed a mono-monostatic body with minimal deviation from the sphere. However, the "Columbus-algorithm" of Section 5 suggests that almost-spherical objects are particularly sensitive to small perturbations of shape, which may often produce *additional* equilibrium points in pitchfork-like or saddle-node bifurcations. So, even if mono-monostatic pebbles exist temporarily, it is very likely that the number of their equilibria is increased even by a small amount of abrasion. While this reasoning implies that pebbles in class {1, 1} are extremely rare, it also tells us that class {2, 2} might be dominant, since it can occur in all four morphology classes.

We conducted a simple statistical experiment: we collected five random samples of 400 pebbles in an area of ca. 15x50 meters along the coast of Rhodes, Greece (Figure 14a). In the first step, convex and non-convex pebbles were separated; their ratio was almost constant 51:49 (Figure 14b). In the second step the convex pebbles were classified according to the scheme of Definition 1 and Definition 3. The number of stable equilibria is relatively easy to identify. We used simple considerations and hand-held experiments to find the number of unstable equilibria. Since the vast majority of the pebbles was

(a) (b)

Fig. 14. (a) View of pebbles on the coast of Rhodes, Greece. (b) Convex (left side) and concave (right side) pebbles in a random sample.

more-or-less *flat*, this was not a very difficult task: by restraining the pebble to roll in its principal plane, saddle points appear to be stable equilibria and are easy to count. Of course, for some pebbles it was impossible to identify to which class $\{i, j\}$ they belonged. The results are summarized in Table 1.

Observe that over 92% of all (over 1,000) convex pebbles have exactly two stable equilibria. The majority of these pieces were rather flat, which can be explained by the back-and-forth sliding motion of the pebbles in the coastal wave current. The small variation in the dominant equivalence classes is remarkable and suggests that a similar table might be characteristic for a given area. Most notably, we did not find *any* monostatic pebbles. Although monostatic pebbles probably exist, they appear to be extremely rare and apparently even more rare are pebbles in class $\{1, 1\}$. Areas with spherical pebbles do exist: the most likely place to find mono-monostatic objects of class $\{1, 1\}$ is probably the surface of Mars. There, hematite was found in the form of spherical grains, also nicknamed "blueberries," which cover large portions of the landscape [20]. It is highly unlikely that Arnold found a spherical object of this kind; his conjecture was probably motivated by mathematical intuition.

Table 1. Statistical results on pebbles collected on the coast of Rhodes, Greece. Data based on five random samples of 400 pebbles each. The empirical expected value and variation are given in percentages for each equivalence class $\{i, j\}$ with i stable and j unstable equilibria.

	j				
i	1	2	3	4	5
1	—	—	—	—	—
2	$0{,}1 \pm 0{,}2\%$	$74{,}5 \pm 2{,}2\%$	$17{,}0 \pm 1{,}9\%$	$1{,}0 \pm 0{,}8\%$	$0{,}1 \pm 0{,}2\%$
3	—	$4{,}5 \pm 2{,}2\%$	$0{,}4 \pm 0{,}4\%$	$0{,}1 \pm 0{,}2\%$	—
4	—	$0{,}2 \pm 0{,}3\%$	—	$0{,}7 \pm 0{,}5\%$	$0{,}1 \pm 0{,}2\%$

Unknown: $1{,}3 \pm 0{,}4\%$

Acknowledgments

Comments from Phil Holmes, Jerry Marsden, Ákos Török, and two unknown referees helped to shape this paper substantially. The authors also thank Réka Domokos for her comments and invaluable help with the pebble experiment. This work has been supported by OTKA grant TS 049885.

Appendix A

Here we prove Lemmas A.1, A.2, and A.3, all of which have been used in the preceding proof of Theorem 2.

A.1. Singular points of R

Here we prove

Lemma A.1. *The function R has no other singular point than the poles.*

Proof of Lemma A.1. The poles are singular points because of the reflection-symmetry of R to the planes $\Theta = 0$ and $\Theta = \pi/2$ (cf. equation (7)).

At other points, the partial derivatives of R are determined based on equations (1) and (8). The first one is

$$\frac{\partial R}{\partial \theta} = d\frac{\partial a}{\partial \theta} \cdot (f_1 - f_2). \tag{11}$$

This partial derivative is zero if either

$$f_2 - f_1 = 0, \tag{12}$$

which holds for the poles only, or

$$\frac{\partial a}{\partial \theta} = 0, \tag{13}$$

which holds if and only if $\theta = k \cdot \pi/2$. At these lines,

$$R(\theta, \varphi) = 1 + d \cdot f_i(\varphi), \qquad i = 1 + k \bmod 2 \tag{14}$$

(cf. equations (5) and (6)). Now we have to show that the second partial derivative is non-zero *along these lines*. The second partial derivative at $\theta = k \cdot \pi/2$ (with respect to φ) is given by

$$\frac{\partial R}{\partial \varphi} = d \cdot \frac{df_i(\varphi)}{d\varphi}, \quad i = 1 + k \bmod 2, \tag{15}$$

which is non-zero except at the poles. Thus, there are really no other singular points. □

A.2. Coincidence of the Origin with the Center of Gravity

In this subsection we show under which conditions the origin O of the coordinate system coincides with the center of gravity G of the body $\mathcal{B}$, defined by the surface R (cf. equations (1)–(8)).

Lemma A.2. *There exist positive constants $c_1 < c_2$, δ_0 and a function F_1 such that for arbitrary $\delta < \delta_0$, $(c, d) = (F_1(\delta), \delta)$ implies $G \equiv O$ and $c_1 \leq F_1(\delta) \leq c_2$.*

Proof of Lemma A.2. The reflection symmetry of the body with respect to the $\theta = 0$ and $\theta = \pi/2$ planes implies that G is on the vertical line $\varphi \pm \pi/2$ passing through the origin O. The vertical distance h between O and G can be expressed as a function of the parameters c and d:

$$h(c, d) = \frac{\int_0^{2\pi} \int_{-\pi/2}^{\pi/2} \frac{1}{4} R(\varphi, \theta, c, d)^4 \cos\varphi \sin\varphi \, d\varphi \, d\theta}{V(c, d)}. \tag{16}$$

where $V(c, d)$ denotes the volume of the body, and $G \equiv O$ iff $h(c, d) = 0$.

Equation (16) can be transformed to

$$\begin{aligned} h(c, d) &= \frac{1}{V(c, d)} \int_0^{2\pi} \int_{-\pi/2}^{\pi/2} \tfrac{1}{4}(1 + d\Delta R(\varphi, \theta, c))^4 \cos\varphi \sin\varphi d\varphi d\theta \\ &= \frac{1}{V(c, d)} \left[\int_0^{2\pi} \int_{-\pi/2}^{\pi/2} \cos\varphi \sin\varphi d\varphi d\theta \right. \\ &\quad \left. + d \int_0^{2\pi} \int_{-\pi/2}^{\pi/2} (\Delta R + \tfrac{3}{2} d\Delta R^2 + d^2 \Delta R^3 + \tfrac{1}{4} d^3 \Delta R^4) \cos\varphi \sin\varphi d\varphi d\theta \right] \\ &= \frac{1}{V(c, d)} \\ &\quad \times \left[0 + d \int_0^{2\pi} \int_{-\pi/2}^{\pi/2} (\Delta R + \tfrac{3}{2} d\Delta R^2 + d^2 \Delta R^3 + \tfrac{1}{4} d^3 \Delta R^4) \cos\varphi \sin\varphi d\varphi d\theta \right], \end{aligned} \tag{17}$$

which shows that $h(c, d) = 0$ is equivalent to the condition

$$h'(c, d) = \int_0^{2\pi} \int_{-\pi/2}^{\pi/2} (\Delta R + \tfrac{3}{2} \, d\Delta R^2 + d^2 \Delta R^3 + \tfrac{1}{4} \, d^3 \Delta R^4) \cos\varphi \sin\varphi \, d\varphi \, d\theta = 0, \tag{18}$$

if $d > 0$; moreover,

$$sign(h(c, d)) = sign(h'(c, d)). \tag{19}$$

We remark that $h'(c, d)$ is continuous in c and d, for $c > 0$ and arbitrary d (d might be 0 as well).

Observe that

$$h'(c, 0) = \int_0^{2\pi} \int_{-\pi/2}^{\pi/2} \Delta R \cos\varphi \sin\varphi d\varphi d\theta \tag{20}$$

is positive if c approaches infinity, because

$$\lim_{c\to\infty} \Delta R(\theta, \varphi, c) = \sin(\varphi), \tag{21}$$

and the product $\Delta R \cos\varphi \sin\varphi$ is nonnegative (see also Figure 9a).

At the same time, if $c \to 0$, we have

$$\lim_{c\to 0} \Delta R(\theta, \varphi, c) = \left\{ \begin{array}{ll} 1 & \text{if} \left\{ \begin{array}{c} -\pi/2 < \varphi < 0,\ \theta \neq k\cdot\pi/2 \\ \varphi = \pi/2 \\ -\pi/2 < \varphi < \pi/2,\ \theta = (2k+1)\cdot\pi/2 \end{array} \right\} \\ -1 & \text{if} \left\{ \begin{array}{c} 0 < \varphi < \pi/2,\ \theta \neq k\cdot\pi/2 \\ \varphi = -\pi/2 \\ -\pi/2 < \varphi < \pi/2,\ \theta = 2k\cdot\pi/2 \end{array} \right\} \\ \sin^2\theta - \cos^2\theta & \text{if} \quad \varphi = 0 \end{array} \right\}, \tag{22}$$

and the product $\Delta R \cos\varphi \sin\varphi$ is typically negative, yielding $h'(c, 0) < 0$ (cf. Figure 9b).

Since $h'(c, 0)$ is continuous in c, there exist positive constants $c_1 < c_2$ such that $h'(c_1, 0) < 0 < h'(c_2, 0)$ (see the lower part of Figure 10). Again, because of the continuity of $h'(c, d)$, there exists a constant δ_0 for which $0 < \delta < \delta_0$ implies $h'(c_1, \delta) < 0 < h'(c_2, \delta)$. So if $0 < \delta < \delta_0$, there is a constant $c_1 < F_1(\delta) < c_2$ for which $h'(c_0, \delta) = 0$. Thus, $c = F_1(\delta)$ and $d = \delta$ implies that $G \equiv O$. □

A.3. Convexity of the Body

In this part we show

Lemma A.3. *There exists a continuous function $F_2(c)$ for any $c > 0$, so that the body is convex if $0 < d < F_2(c)$.*

We prepare the proof of Lemma A.3 in four parts.

In Section A.3.1, a sufficient condition of local convexity is determined, based on the Hessian of the surface in a local orthogonal coordinate system. This condition can be applied everywhere except the poles. In Section A.3.2, some functions related to R are extended to a closed domain and their boundedness is stated in Proposition A.3.2. Based on these results, in A.3.3 we prove Proposition A.3.3, stating convexity at regular points (we determine a function $F_2(c)$ and show that the surface is convex at such points if $d < F_2(c)$). Finally, it is verified in Section A.3.4 that the convexity requirement is fulfilled at the poles, too; this is the statement of Proposition A.3.4.

Proof of Lemma A.3. Propositions A.3.3 and A.3.4 imply Lemma A.3. □

A.3.1. A Sufficient Condition for Local Convexity at an Arbitrary Point. At any surface point $P(\varphi_0, \theta_0)$, R can be expressed as $z(x, y)$ in an x-y-z local orthogonal coordinate system, axis z passes through the origin O (see Figure 15). A sufficient

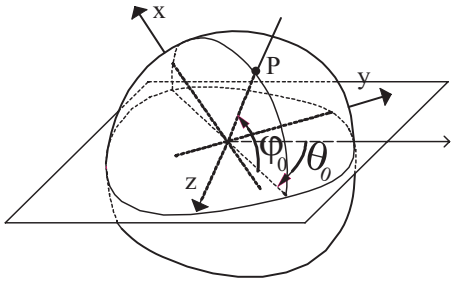

Fig. 15. A local coordinate system at point P of the surface.

condition of local convexity is that the Hessian

$$\mathbf{H} = \begin{bmatrix} z_{xx}(c,d) & z_{xy}(c,d) \\ z_{yx}(c,d) & z_{yy}(c,d) \end{bmatrix} \tag{23}$$

of $z(x, y)$ exists and it is positive definite. Hence $z_{xy} = z_{yx}$, and this condition is the equivalent of

$$\begin{cases} z_{xx}(c,d) > 0, \\ z_{xx}(c,d) z_{yy}(c,d) - z_{xy}(c,d)^2 > 0. \end{cases} \tag{24}$$

(25)

The elements of the Hessian can be expressed as functions of φ and θ. The following results were computed analytically for a general function of the form (1), using Maple 7. The computational details are omitted here. Lower indices in the following equations denote derivatives with respect to the variables in the indices:

$$z_{xx} = \frac{1}{R} - \frac{d \cdot \Delta R_{\varphi\varphi}}{R^2} + \frac{2d^2 \cdot \Delta R_{\varphi}^2}{R^3}, \tag{26}$$

$$z_{yy} = \frac{1}{R} - \frac{d \cdot \Delta R_{\varphi\varphi}}{R^2 \cos^2\varphi} + \frac{2d^2 \cdot \Delta R_{\theta}^2}{R^3 \cos^2\varphi} + \frac{d \cdot \Delta R_{\varphi} \sin\varphi}{R^2 \cos\varphi}, \tag{27}$$

$$z_{xy} = \frac{d \cdot \Delta R_{\theta\varphi}}{R^2 \cos\varphi} + \frac{d \cdot \Delta R_{\theta} \sin\varphi}{R^2 \cos^2\varphi} - \frac{2d^2 \cdot \Delta R_{\varphi} \Delta R_{\theta}}{R^3 \cos^2\varphi}. \tag{28}$$

The above three formulae, substituted in equations (24) and (25), yield a sufficient condition of local convexity of the surface R. It can be used anywhere but at the two poles, where the surface is not twice differentiable.

A.3.2. Boundedness of Some Functions Related to *R*. Here we show

Proposition A.3.2. *There exists a positive continuous function M(c) satisfying the following two conditions:*

$$|\Delta R_{\varphi\varphi}(-\pi/2, \pi/2)| < M, \tag{29}$$

$$\left|\frac{\Delta R_\varphi}{\cos\varphi}\right|, \left|\frac{\Delta R_\theta}{\cos^2\varphi}\right|, |\Delta R_{\varphi\varphi}|, \left|\frac{\Delta R_{\varphi\theta}}{\cos\varphi}\right|, \left|\frac{\Delta R_{\theta\theta}}{\cos^2\varphi}\right| \; < \; M \quad \textit{if} \quad |\varphi| < \pi/2. \tag{30}$$

We can trivially satisfy (29), but there is no such guarantee for the boundedness of the left side of (30), since these are continuous functions on open domains*; observe also that the denominators* $\cos\varphi$ *of (30) converge to zero at the borders of the domains.*

Proof of Proposition A.3.2. Let us define $\mathrm{ext}(\phi)$ for a given function $\phi(\varphi, \Theta)$ with $|\varphi| < \pi/2$ as the same function on an extended, *closed* domain:

$$\mathrm{ext}(\phi) = \begin{cases} \phi(\varphi, \Theta), & \text{if } \; |\varphi| < \pi/2, \\ \lim\limits_{\varphi\to\pi/2} \phi(\varphi, \Theta), & \text{if } \quad \varphi = \pi/2, \\ \lim\limits_{\varphi\to-\pi/2} \phi(\varphi, \Theta), & \text{if } \; \varphi = -\pi/2. \end{cases} \tag{31}$$

The following functions

$$\mathrm{ext}\left(\frac{\Delta R_\varphi}{\cos\varphi}\right), \mathrm{ext}\left(\frac{\Delta R_\theta}{\cos^2\varphi}\right), \mathrm{ext}(\Delta R_{\varphi\varphi}), \mathrm{ext}\left(\frac{\Delta R_{\varphi\theta}}{\cos\varphi}\right), \mathrm{ext}\left(\frac{\Delta R_{\theta\theta}}{\cos^2\varphi}\right) \tag{32}$$

trivially exist and are continuous in φ and θ if $|\varphi| < \pi/2$. Simultaneously, for $|\varphi| < \pi/2$, one can determine the functions in (32) analytically, based on the definition (31) to verify the same statement.

According to our analytical computations (made with Maple 7), the corresponding limit values exist and they are continuous in θ, which imply the continuity of the extended functions (32). Because the results are quite lengthy, only one of them is presented here:

$$\begin{aligned} \mathrm{ext}\left(\frac{\Delta R_\varphi}{\cos\varphi}\right)\Bigg|_{\varphi=+\pi/2} &= \lim_{\varphi\to\pi/2} \frac{\Delta R_\varphi}{\cos\varphi} \\ &= \frac{\cos^2\theta\cdot e^{4/c} + 1 - \cos^2\theta}{\begin{array}{l} c^2(e^{2/c} - 2e^{1/c} + 1 + \cos^2\theta\cdot e^{4/c} \\ -2\cos^2\theta\cdot e^{3/c} + 2\cos^2\theta\cdot e^{1/c} - \cos^2\theta) \end{array}}. \end{aligned} \tag{33}$$

The denominator is never zero:

$$\begin{aligned} 1 \; &+ \; \cos^2\theta\cdot e^{4/c} - 2\cos^2\theta\cdot e^{3/c} + 2\cos^2\theta\cdot e^{1/c} - \cos^2\theta - 2e^{1/c} \\ &= \; 1 + \cos^2\theta\cdot(e^{4/c} - 2e^{3/c} + e^{2/c}) + 2\cos^2\theta\cdot e^{1/c} - \cos^2\theta - 2e^{1/c} + \sin^2\theta\cdot e^{2/c} \\ &> \; 1 + 2\cos^2\theta\cdot e^{1/c} - \cos^2\theta - 2e^{1/c} + \sin^2\theta\cdot e^{2/c} \\ &= \; \sin^2\theta(e^{2/c} - 2e^{1/c} + 1) > 0, \end{aligned} \tag{34}$$

therefore function exists and it is continuous in θ. □

According to the Extreme Value Theorem [22], continuous functions on compact manifolds are always bounded. Thus, the maximum $M(c)$ of all the functions in (32) exists. $M(c)$ satisfies the conditions (29) and (30) and it is continuous in c.

A.3.3. The Function $F_2(c)$. Here we construct the function $F_2(c)$ such that whenever $d < F_2(c)$, R is convex at all regular points. Subsection A.3.4 extends this result to the poles.

Proposition A.3.3. *If*

$$d \le F_2(c) = \min\left\{\frac{1}{25M(c)}, \frac{1}{2}\right\} \tag{35}$$

(where $M(c)$ is defined in Proposition A.3.2), then R is convex at all regular points.

Proof of Proposition A.3.3. Consider the following approximations on the elements of the Hessian (26)–(28), using Proposition A.3.2 and (35) (observe that (35) implies $1/2 < R < 3/2$):

$$\begin{aligned}
z_{xx} &\ge \frac{1}{R} - \left|\frac{d\cdot\Delta R_{\varphi\varphi}}{R^2}\right| + 0 > \frac{2}{3} - 4dM, &(36)\\
z_{yy} &\ge \frac{1}{R} - \left|\frac{d\cdot\Delta R_{\theta\theta}}{R^2\cos^2\varphi}\right| + 0 - \left|\frac{d\cdot\Delta R_{\varphi}\sin\varphi}{R^2\cos\varphi}\right|\\
&> \frac{2}{3} - 4dM - 4dM\cdot\sin\varphi > \frac{2}{3} - 8dM,\\
|z_{xy}| &\le \left|\frac{d\cdot\Delta R_{\theta\varphi}}{R^2\cos\varphi}\right| + \left|\frac{d\cdot\Delta R_{\theta}\sin\varphi}{R^2\cos^2\varphi}\right| + \left|\frac{2d^2\cdot\Delta R_{\varphi}\Delta R_{\theta}}{R^3\cos^2\varphi}\right|\\
&< 4dM + 4dM\sin\varphi + 16d^2M^2\cdot\cos\varphi &(37)\\
&\le 3dM + 16d^2M^2. &(38)
\end{aligned}$$

From inequalities (35)–(38), we have

$$z_{xx}(d) > \frac{2}{3} - 4dM \ge \frac{38}{75} > 0, \tag{39}$$

and

$$\begin{aligned}
z_{xx}(d)z_{yy}(d) - z_{xy}(d)^2 &> (\tfrac{2}{3} - 4dM)(\tfrac{2}{3} - 8dM) - (8dM + 16d^2M^2)^2\\
&\ge \frac{28\cdot 7057}{3^2\cdot 5^8} > 0, &(40)
\end{aligned}$$

i.e., the conditions of convexity (24), (25) are satisfied; the function $F_2(c)$ is continuous in c. □

A.3.4. Convexity at the Poles. In this part, we prove

Proposition A.3.4. *$\mathcal{B}$ is locally convex at the two poles if $d < F_2(c)$.*

Here, local convexity is demonstrated by showing a plane, which

- contains the examined pole (N or S),
- has all nearby points of the surface on the same side of the plane,
- has the "inside" of $\mathcal{B}$ also on the same side of the plane. (We choose the origin O, which is always an inner point of the body, to examine this condition.)

Proof of Proposition A.3.4. Consider the orthogonal coordinate system of Figure 15 with $\varphi_0 = -\pi/2$ and $\theta_0 = 0$. The plane $z = (1 + d)$ contains the north pole of the surface and all other points are on the $z < 1 + d$ side of this plane, because

$$Z(\varphi, \theta) = R(\varphi, \theta) \sin\varphi < R(\varphi, \theta) < 1 + d. \tag{41}$$

The origin O is at $z = 0$ also on the $z < 1 + d$ side. Thus, the surface is convex at the north pole for any value of d.

Similarly, the plane $z = -1 + d$ contains the south pole, and the origin O is at $z = 0$ on the $z > -1 + d$ side. The surface is locally convex if

$$z(\varphi, \theta) = R(\varphi, \theta) \sin\varphi > -1 + d, \tag{42}$$

for any θ if $0 < \varphi + \pi/2 \ll 1$ and $d < F_2(c)$.

We start the proof of inequality (42) with the following simple relation, which is true for arbitrary positive M (see also (35)):

$$d \le \min\left\{\frac{1}{25M}, \frac{1}{2}\right\} < \frac{2}{3(1+M)}. \tag{43}$$

We increase the right side of this inequality in three steps, which are discussed below:

$$\begin{aligned} d < \frac{2}{3(1+M)} &= \frac{\frac{1}{3}(\varphi+\pi/2)^2}{\frac{1}{2}(1+M)(\varphi+\pi/2)^2} < \frac{\frac{1}{3}(\varphi+\pi/2)^2}{\frac{1}{2}(1+M)(\varphi+\pi/2)^2 - \frac{1}{4}M(\varphi+\pi/2)^4} \\ &= \frac{1 - 1 + \frac{1}{3}(\varphi+\pi/2)^2}{1 - (-1 + \frac{1}{2}M(\varphi+\pi/2)^2)(-1 + \frac{1}{2}(\varphi+\pi/2)^2)} \\ &< \frac{1+\sin\varphi}{1 - (-1 + \frac{1}{2}M(\varphi+\pi/2)^2)\sin\varphi} \\ &< \frac{1+\sin\varphi}{1 - \Delta R \sin\varphi}. \end{aligned} \tag{44}$$

The first step was obvious. In the second step we used that

$$-1 + \frac{1}{3}(\varphi+\pi/2)^2 < \sin\varphi < -1 + \frac{1}{2}(\varphi+\phi/2)^2, \tag{45}$$

if $0 < (\varphi + \pi/2) \ll 1$, which is simple to derive from the Taylor expansion of $\sin(\varphi)$ at $\varphi = -\pi/2$ up to the third-order term. The third step is a consequence of (cf. Figure 7

and eq. (29))

$$\begin{aligned}\Delta R(\varphi,\theta) &\le f_2(\varphi) = \Delta R(\varphi,\pi/2)\\ &= -1 + 0\cdot(\varphi+\pi/2) + \tfrac{1}{2}R_{\varphi\varphi}(-\pi/2,\pi/2)\cdot(\varphi+\pi/2)^2 + o((\varphi+\pi/2)^3)\\ &< -1 + \tfrac{1}{2}M(\varphi+\pi/2)^2, \end{aligned} \tag{46}$$

which again holds for $0 < (\varphi + \pi/2) \ll 1$.

Eq. (44) can be rearranged as

$$d(1 - \Delta R\sin\varphi) < 1 + \sin\varphi. \tag{47}$$

Via substituting eq. (1) into (47), we get eq. (42). Thus, the surface is convex at the south pole, too. □

Appendix B: The Planar Results and the Four-Vertex Theorem

In this appendix we show the following:

Lemma B.1. *The 4V Theorem and Theorem 1 are equivalent.*

As demonstrated in [1] and already mentioned in the introduction, Theorem 1 has another equivalent form.

Theorem 1A. *Let the function $r(\alpha) > 0$ with isolated extrema, $0 \le \alpha \le 2\pi$ and $r(0) = r(2\pi)$, determine a planar curve in a polar coordinate system (r,α). If the center of gravity G of the corresponding planar* solid body *is at the origin $(0,0)$, the function $r(\alpha)$ has at least four extrema. This statement holds for concave curves, too.*

One possible interpretation of Theorem 1A is the following: Consider a coordinate system (x, y) so that $G(x_G, y_G)$ is at the origin $(0, 0)$ (Figure 16a). Theorem 1A determines the minimal number of local extrema of the function $r(\alpha)$ under the following additional integral constraints:

$$y_G = \int_{\substack{area\\ of\ the\\ body}} y\,dA = \tfrac{1}{3}\int_0^{2\pi} r^3(\alpha)\cos(\alpha)\,d\alpha = 0, \tag{48}$$

$$x_G = \int_{\substack{area\\ of\ the\\ body}} x\,dA = \tfrac{1}{3}\int_0^{2\pi} r^3(\alpha)\sin(\alpha)\,d\alpha = 0. \tag{49}$$

Now we will show that the 4V theorem can be formulated in an analogous manner.

Consider a strictly convex, closed, planar curve of length $l = 2\pi$ (Figure 16b). Let $0 \le s \le 2\pi$ denote the arclength of the curve (measured clockwise from point S). Let $x(s)$ and $y(s)$ denote orthogonal coordinates of the points of the curve. Let $\beta(s_0)$ be the angle of the clockwise-oriented tangent of the curve at $s = s_0$ (with $\beta(0) = 0$ and

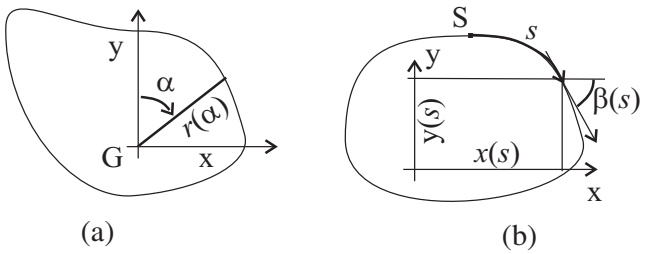

Fig. 16. (a) A planar body in the polar coordinate system. (b) A convex, closed plane curve.

$\beta(2\pi) = 2\pi$), and let $\rho(s_0)$ denote the curvature of the curve at the same point. Since the curve is strictly convex ($\rho(s) > 0$), $\beta(s)$ is strictly monotonically increasing, implying the existence of $s(\beta)$ and $\rho(\beta)$ for $0 \leq \beta \leq 2\pi$. From the monotonicity of $\beta(s)$ it also follows that $d\rho/ds = 0$ implies $d\rho/d\beta = 0$ and vice versa.

The 4V theorem (analogously to Theorem 1a) states that the number of local extrema of the function $\rho = d\beta/ds$ is at least four. The closing condition for the curve yields the following integral constraints:

$$\begin{aligned} x(2\pi) - x(0) &= \int_0^{2\pi} \frac{dx}{ds}\, ds = \int_0^{2\pi} \cos(\beta(s))\, ds \\ &= \int_{\beta(0)}^{\beta(2\pi)} \frac{\cos(\beta)}{d\beta/ds}\, d\beta = \int_0^{2\pi} \frac{\cos(\beta)}{\rho(\beta)}\, d\beta = 0, \end{aligned} \tag{50}$$

$$\begin{aligned} y(2\pi) - y(0) &= \int_0^{2\pi} \frac{dy}{ds}\, ds = \int_0^{2\pi} \sin(\beta(s))\, ds \\ &= \int_{\beta(0)}^{\beta(2\pi)} \frac{\sin(\beta)}{d\beta/s}\, d\beta = \int_0^{2\pi} \frac{\sin(\beta)}{\rho(\beta)}\, d\beta = 0. \end{aligned} \tag{51}$$

Equations (48)–(49) and (50)–(51) are equivalent if

$$\rho(\beta) = \frac{1}{r^3(\alpha)}, \tag{52}$$

which is a mutually one-to-one correspondence between the positive, periodic functions $r(\alpha)$ and $\rho(\beta)$ ($\alpha, \beta \in [0, 2\pi]$), determining homogeneous planar bodies and convex plane curves, respectively.

As we can see, for convex curves the 4V theorem is equivalent to the fact that $1/r^3(\alpha)$ has four extrema. The latter coincide with the extrema of $r(\alpha)$; thus the 4V theorem for convex curves and Theorem 1 are equivalent. □

References

[1] Domokos, G., Papadopulos, J., and Ruina, A., Static equilibria of planar, rigid bodies: Is there anything new? *J. Elasticity* **36** (1994), 59–66.

[2] Berger, M., and Gostiaux, B., *Differential geometry: Manifolds*, *curves and surfaces* (1988), Springer, New York.
[3] Conway, J. H., and Guy, R., Stability of polyhedra, *SIAM Rev.* **11** (1969), 78–82.
[4] Dawson, R., Monostatic simplexes, *Amer. Math. Monthly* **92** (1985), 541–646.
[5] Dawson, R., and Finbow, W., What shape is a loaded die?, *Mathematical Intelligencer* **22** (1999), 32–37.
[6] Heppes, A., A double-tipping tetrahedron, *SIAM Rev*. **9** (1967), 599–600.
[7] Nowacki, H., Archimedes and ship stability. In: *Passenger ship design, construction, operation and safety*: Euroconference; Knossos Royal Village, Anissaras, Crete, Greece, October 15–17, 2001, 335–360 (2002). Ed: Kaklis, P.D. National Technical Univ. of Athens, Department of Naval Architecture and Marine Engineering, Athens.
[8] Wikipedia, Dice, http://en.wikipedia.org/wiki/Dice
[9] Arnold, V.I., *Ordinary differential equations*, 10th printing (1998), MIT Press, Cambridge.
[10] Farkas, M., *Periodic motions* (1994), Springer, New York.
[11] Champneys, A.R., and Fraser, W.B., The "Indian rope trick" for a parametrically excited flexible rod: I linearised analysis, *Proc. Roy. Soc. Lond. A* **456** (2000), 553–570.
[12] Enikov, E., and Stépán, G., Digital stabilization of unstable equilibria, *Zeitschrift für angewandte Mathematik und Mechanik* **75** (1995), S111–S112.
[13] Goodwine, B., and Stépán, G., Controlling unstable rolling phenomena, *J. Vibration and Control* **6** (2000), 137–158.
[14] Bloch, A.M., Marsden, J.E., and Zenkov, D.V., Nonholonomic dynamics, *Not. Amer. Math. Soc.* **52** (2005), no. 3, 324–333.
[15] Borisov, A.V., and Mamaev I.S., The rolling motion of a rigid body on a plane and a sphere: hierarchy of dynamics, *Reg. Chaot. Dynam.* **7** (2002), no. 2, 177–200.
[16] Chaplygin, S.A., On the rolling of a sphere on a horizontal plane, *Mat. Sbornik* **XXIV** (1903), 139–168 (in Russian).
[17] Arnold, V.I., Personal communication to G. Domokos.
[18] Blatt, H., Middleton, G., and Murray, R., *Origin of sedimentary rocks* (1972), Prentice Hall, Englewood Cliffs, NJ.
[19] Chamley, H., *Sedimentology* (1990), Springer, New York.
[20] Squyres, S., et al., The opportunity rover's Athena science investigation at Meridiani Planum, Mars, *Science*, **306** (2004), 1698–1703.
[21] Avrin, J., Global existence and regularity for the Lagrangian averaged Navier-Stokes equations with initial data in H-1/2, *Commun. Pure Appl. Anal.* **3** (2004), no. 3, 353–366.
[22] Malik, S. C., *Mathematical analysis*, 2nd ed. (1992), Wiley, New York.